An ultrasensitive and universal surface plasmonic biosensor for detection of micropollutants in aquatic environments

Jisui Tan[a,1], Zongren Dai[b,1], Kaiming Zhou[c], Lin Zhang[c], Miao He[a], Yidong Tan[b*] and Xiaohong Zhou[a*]

a State Key Joint Laboratory of ESPC, School of Environment, Tsinghua University, Beijing 100084, China

b State Key Laboratory of Precision Measurement Technology and Instruments, Department of Precision Instrument, Tsinghua University, Beijing 100084, China

c Aston Institute of Photonic Technologies, Aston University, Birmingham B4 7ET, UK

1 These authors contributed equally to this work

*Corresponding authors: xhzhou@mail.tsinghua.edu.cn (Xiaohong Zhou); Tanyd@mail.tsinghua.edu.cn (Yidong Tan)

ABSTRACT

Simple and yet ultrasensitive and accurate quantifying a variety of analytical targets by virtue of a universal sensing device holds promise to revolutionize environmental monitoring, medical diagnostics, and food safety. Here, we propose a novel optical surface plasmon resonance (SPR) system in which the frequency-shifted light of different polarization returned the laser cavity to stimulating laser heterodyne feedback interferometry (LHFI), hence amplifying the reflectivity change caused by the refractive index (RI) variations on the gold-coated SPR chip surface. In addition, the *s*-polarized light further used as the reference to compensate the noise of the LHFI-amplified SPR system, resulting in nearly 3 orders of magnitude enhancement of RI resolution (5.9×10^{-8} RIU) over the original SPR system (2.0×10^{-5} RIU). By exploiting nucleic acids, antibodies, and receptors as recognition materials, a variety of micropollutants are detected with ultra-low detection limits, ranging from a toxic metal ion (Hg^{2+}, 70 ng/L), to a group of commonly occurring biotoxin (microcystins, 3.9 ng microcystin-LR/L), and to a class of environmental endocrine disruptors (estrogens, 0.7 ng 17β-estradiol/L). This sensing platform exhibits several distinct characteristics, including dual improvement of sensitivity and stability, and common-path optical construction without needing optical alignment, demonstrating a promising avenue towards environmental monitoring.

KEYWORDS

Environmental monitoring; Surface plasmon resonance; Laser heterodyne feedback; Polarized light compensation; Biosensor; Ultrasensitive detection

SYNOPSIS

An OLFM-compensated and LHFI-amplified SPR biosensor for ultrasensitive detection of a variety of analytical targets with universality.

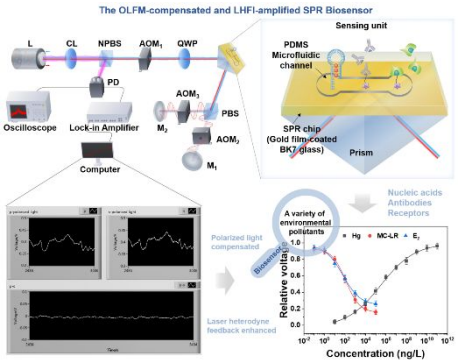

For TOC

INTRODUCTION

Precise and reliable monitoring micropollutants of widespread concern in aquatic environment, is of great significance for the risk assessments of public safety and ecological health. Traditional analytical devices, such as high-performance liquid chromatography (HPLC), and gas chromatography−mass spectrometry (GC−MS), are greatly limited in sensitivity and universality, especially compounds that have not been previously recognized. Therefore, developing a universal biosensing platform with excellent sensitivity and stability, to quantify and assess a broad range of analytical targets is in high demand for environmental monitoring.

Significant advances have been witnessed in the use of various biological recognition material-based schemes to detect analytical targets, such as antibodies,[1] functional nucleic acids,[2] and receptors[3] recent years. Among these, one of the most successful and commonly used schemes is refractive index (RI)-based label-free optical biosensing and the biosensors developed therefrom have been exploited for a broad range of applications due to their excellent performance, such as easy-to-operation and showing enormous potential for miniaturization and for simultaneous quantification of multiplexed analytical targets.[4] Surface plasmons are electromagnetic excitations that propagate along an interface between metal and dielectric medium, consisting of an interface-bound evanescent wave in the dielectric and medium charge density oscillations in the metal.[5] As a typical RI-based label-free optical biosensor, conventional intensity-modulated surface plasmon resonance (SPR) system based on prism coupling has been widely reported, generally exhibiting a RI resolution of 10^{-5}

RIU.[6]

Although various sensitivity enhancement schemes have been exploited building on the basic structure of SPR, such as optimizing the SPR-coated layer,[7] utilizing phase or angular modulation,[8] and adding a nanodielectric layer,[9] they have trade-offs among sensitivity, simplicity, stability, and cost. As an alternative, the laser heterodyne feedback interferometry (LHFI) makes the feedback weak optical signal participate in the stimulated radiation of the laser for spontaneous amplification, that can be leveraged for intensity-modulated SPR sensitivity enhancement. More specifically, the frequency-shifted incident light senses, and then partially returns to the laser cavity, in turn resonating with the relaxation oscillation and inducing the intensity modulation of the laser; as a consequence, the modulated output of the laser can be enhanced even up to 10^6-fold compared with the feedback one.[10, 11] In this scheme, the laser source acts as an emitter, responder, and intrinsic amplifier simultaneously, which does rarely need optical alignment and reduces optical components required. Because of its compactness, self-collimation, and sensitivity, the LHFI has been widely explored for displacement sensing,[12] particle detection,[13] confocal tomography[14] and so on. Despite of its promise, enhanced sensitivity to SPR via the LHFI is rarely reported so far. Besides, the inherent noise caused by the air disturbance and the laser is an unavoidable problem in the label-free SPR sensing.

To address the challenge, we exploited a polarized light-compensated SPR system with laser heterodyne feedback for ultrasensitive detection of a various of analytical targets. In this platform, the LHFI was adopted to remarkably amplify the intensity change

caused by the molecular/biomolecular binding-induced RI variations when the SPR was excited on the surface. Inspired by the common-path compensation reports via frequency multiplexing[15] or polarized light,[16] we further proposed a common-path compensation approach combining the orthogonally-polarized light with frequency multiplexing (OLFM) to minimize the impact of mechanical, thermal, and laser noise, which was compatible with the SPR system and significantly improved the stability of this system. Subsequently, the strategy to anchor functional groups/molecules on the SPR chip was realized by forming self-assembled monolayers (SAMs) spontaneously on gold film via the Au-S bond. As proof-of-concept demonstrations, we adopted this technique for specifically detecting mercury ions (II) (Hg^{2+}), broad-spectrum immunoassay of microcystins (MCs), and screening of estrogenic binding activity in environmental samples and achieved ultralow detection limits.

MATERIALS AND METHODS

Experimental Procedures

Detailed information on materials and reagents were provided in the Supporting Information (**Note S1**).

Experimental setup. The OLFM-compensated and LHFI-amplified SPR system was excited by using a home-made 1064 nm solid-state microchip laser. The incident angle was controlled via an electric turntable (Micronix Inc., PR-50-11300) attached to the sensing unit with a resolution of 5 microdegrees and a scanning range from 0 to 360 degrees. The sensing unit of this system was composed of a microfluidic channel (9 × 6 mm in area and 1 mm in depth) made of polydimethylsiloxane (PDMS) and a SPR chip

on the prism (Daheng Optics Inc., GCL-030102A). The SPR chip was made of a BK7 glass slide (20 × 20 mm in area and 1 mm in depth) coated with 2 nm chromium adhesion layer and 52 nm gold film by using an electron-beam evaporator (Canon-Anelva Inc., L-400EK). The *p*- and *s*-polarized beams were frequency shifted by three AOMs (Castech Inc., CAFS-70-3-020-TEC-1064-AF). The modulated light was acquired by using a PD (Thorlabs Inc., PDA20CS2) with a lock-in amplifier (Zurich Instrument Inc., HF2LI). Different samples were injected in the microfluidic channel at a constant flow velocity of 100 μL/min by a syringe pump (Longer Inc., LSP01-2A). The SPR signal responses during the detection process were ultimately acquired by using a PD with a lock-in amplifier and recorded online and in real-time by LabView software.

Statistical Information. Statistical analysis was performed using Origin 2022. The four-parameter logistic model with unfixed lower and upper boundaries was adopted for curve-fitting. Error bars in all figures represent the standard deviations of three individual experiments in parallel and the blue dotted lines represent the 95% confidence band.

RSULTS AND DISCUSSION

OLFM-compensated and LHFI-amplified SPR Detection Principle. To achieve the sensitivity and stability enhancement to SPR, we designed a novel optical structure in which the frequency-shifted light of different polarization returned to the laser cavity to stimulate LHFI and the *s*-polarized light used as the reference to compensate the noise of the LHFI-amplified SPR system (**Figure 1a** and **Figure S1**). More specifically, the output light of the laser was separated into two parts by a non-polarized beam splitter

(NPBS). The transmitted beam was adjusted to circularly polarized light by a quarter-wave plate (QWP) and then incident on the gold film of the SPR chip. After passing through the sensing unit, the circularly polarized light was divided into *p*- and *s*-polarized light by a polarized beam splitter (PBS). Both of them were frequency shifted differently and reflected by two mirrors (M_1 and M_2), respectively. The feedback beams returned to the laser cavity along the original path, hence inducing the intensity modulation of the laser. The modulated laser power output caused by the two feedback beams can be described as:[17, 18]

$$\frac{\Delta I_p(\Omega_p)}{I} = \kappa_p G(\Omega_p)\cos\left(2\pi\Omega_p t - \phi_{fp} + \phi_{ep}\right)$$

$$\frac{\Delta I_s(\Omega_s)}{I} = \kappa_s G(\Omega_s)\cos\left(2\pi\Omega_s t - \phi_{fs} + \phi_{es}\right)$$

where ΔI_p and ΔI_s are the feedback light-induced intensity modulation of *p*-polarized beam and *s*-polarized beam, respectively; Ω_p and Ω_s are the shift frequencies of the two beams; I denotes the stationary laser intensity; κ_p and κ_s are the coefficients of the feedback strength of the two beams; ϕ_{fp} and ϕ_{fs} are the fixed phases of the two beams; ϕ_{ep} and ϕ_{es} are the external phases of the two beams; $G(\Omega_p)$ and $G(\Omega_s)$ are the frequency-dependent gain factors. To compensate the intensity drift induced by air disturbance, laser and other inherent mechanical and thermal noise, we defined $\Delta I=\Delta I_p-\Delta I_s$ as the corrected intensity change corresponding to the RI variations. The light intensity was ultimately acquired by using a photodiode (PD) with a lock-in amplifier and recorded in the form of voltage by a computer.

To obtain a larger gain factor $G(\Omega_i)$ and demodulate the *p*- and *s*-polarized beams

separately, three acousto-optic modulators (AOMs) were employed, in which AOM_2 and AOM_3 were set with different working frequencies (**Figure 1b**). The frequency-dependent gain factor $G(\Omega_i)$ can be expressed as:[18, 19]

$$G(\Omega_i) = 2\gamma_c \frac{(\eta^2\gamma^2 + 4\pi^2\Omega_i^2)^{1/2}}{[4\eta^2\gamma^2\pi^2\Omega_i^2 + (4\pi^2 f_r^2 - 4\pi^2\Omega_i^2)^2]^{1/2}}$$

where γ_c is the photon decay rate inside the laser cavity, γ is the population inversion decay rate, f_r denotes the frequency of relaxation oscillation, η is the normalized pumping rate, Ω_i (i=p or s) is the shift frequency of p- or s-polarized beam, respectively.

Simulated by MATLAB, we found that the closer to the frequency of relaxation oscillation f_r in our system the shift frequency Ω_p and Ω_s are, the larger the frequency-dependent gain factors $G(\Omega_p)$ and $G(\Omega_s)$ are (blue line in **Figure 1c**). However, when the shift frequency (Ω_p or Ω_s) and frequency of relaxation oscillation f_r were too close, it would cause a state of chaos in the spectrum due to the strong nonlinear effect, which is not conducive to the extraction and demodulation of the two feedback beams. Based on the above considerations, the shift frequency Ω_p and Ω_s were set to be 2 MHz and 3 MHz, respectively, enabling the gain factor $G(\Omega_p)$ and $G(\Omega_s)$ of our system reaching 10^4. Considering that the working frequency of one single AOM was not able to be as low as a few megahertz to meet the conditions set above; thus, we employed two AOMs to acquire a low shift frequency for one optical beam. Specifically speaking (**Figure 1b**), the light with frequency f_0 occurred the positive first order diffraction by AOM_1, resulting that the frequency changed to $f_0+\omega_1$ (ω_1=70 MHz was AOM_1's working

frequency). After split by PBS, the frequency $f_0+\omega_1$ of the *p*-polarized light converted to $f_0+\omega_1-\omega_2$ by the negative first order diffraction under the modulation of AOM_2 (ω_2=71 MHz was AOM_2's working frequency). Finally, the *p*-polarized light returned to the laser cavity by a mirror (M_1) along the original path, accompanying that the frequency changed to $f_0+\omega_1-\omega_2-\omega_2+\omega_1=f_0+\Omega_p=f_0+2$MHz by the combined diffractions of AOM_2 and AOM_1. As similar as the *p*-polarized light, the *s*-polarized light split by PBS shared the differential frequency shift process by setting the working frequency of AOM_3 (ω_3) to be 71.5 MHz, indicating that the *s*-polarized light had a frequency of $f_0+\omega_1-\omega_3-\omega_3+\omega_1=f_0+\Omega_s=f_0+3$MHz. To verify the accuracy of the simulations, we measured the power spectrum of the system and found the Ω_p and Ω_s to be 2 MHz and 3 MHz, respectively, which were absolutely in accordance with simulations (red line in **Figure 1c**).

In the SPR system, a higher sensitivity corresponds to a larger reflectivity change for a certain RI variation, in which the reflectivity change is affected substantially by the incident angle and the gold film thickness of the SPR chip.[20] Calculated by the transfer matrix method (**Note S2**), we found that the reflectivity change reached the maximum 0.237 under the optimal incident angle of 64.01° and the gold film thickness of 52 nm (**Figure 1d**). To further verify the accuracy of the simulations, we set the thickness of gold film at 52 nm and measured the reflectivity curves in pure water, phosphate buffered saline solution and Tris-HCl buffer solution at the incident angles varying from 63° to 67°. As expected, the measured reflectivity curves in three types of solutions were in good agreement with the simulated results (**Figure 1e**). Therefore, to achieve the

maximum sensitivity, the incident angle and gold film thickness were set to be 64.01° and 52 nm, respectively.

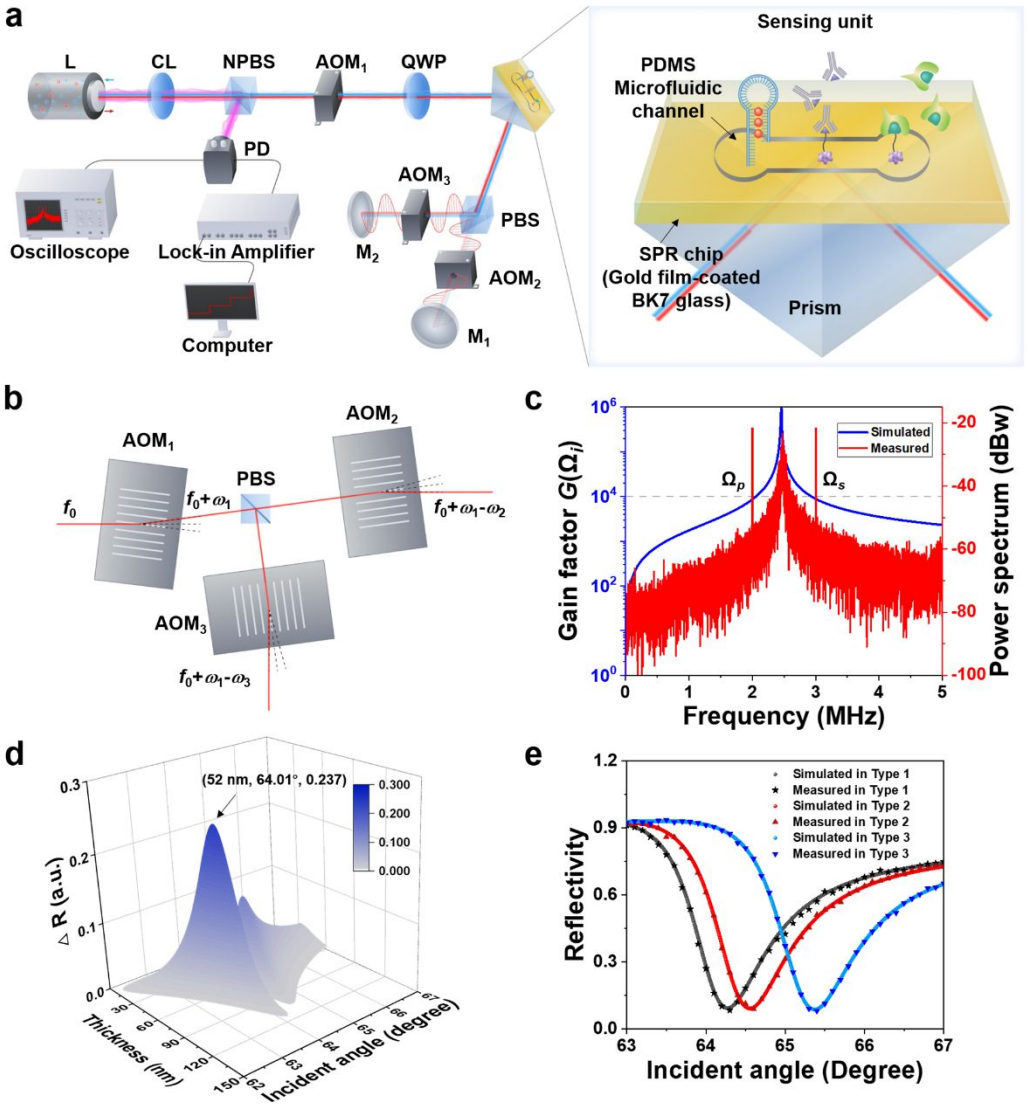

Figure 1 Detection principle. (a) Experimental setup of the OLFM-compensated and LHFI-amplified SPR biosensing platform. L: laser; CL: collimating lens; NPBS: non-polarized beam splitter; AOM_i (i=1, 2, 3): acousto-optic modulator; QWP: quarter-wave plate; PBS: polarized beam splitter; M_i (i=1, 2): mirror; PD: photodiode; (b) Schematic three AOMs-based differential frequency shift module diagram; (c) Simulated gain factor varying with different shift frequency (blue line) and experimentally measured

power spectrum of the system (red line); (d) Simulated reflectivity changes with gold film thickness and incident angle under the condition of RI variation of 0.002; (e) Relationship between reflectivity and incident angle under the condition of gold film thickness of 52 nm. Type 1 referred to water (n=1.3242), Type 2 referred to phosphate buffered saline solution (n=1.3272), and Type 3 referred to Tris-HCl buffer solution (n=1.3357).

Performance Evaluation for RI Sensitivity. To confirm the stability of the LHFI-amplified SPR system with OLFM compensation approach, we monitored the voltage drift of the measurement channel of *p*-polarized light and the compensation channel of *s*-polarized light, separately (**Figure 2a** and **Movie 1**). We found that the baseline fluctuations responding to water in the *p*-polarized and *s*-polarized light path were relatively large in the 3-hour testing, however, the corrected signal (U=U_p-U_s) was significantly improved with stability than that of the measurement channel (U_p) and compensation channel (U_s), indicating the reliability of OLFM compensation approach in minimizing the impact of inherent noise of LHFI-amplified SPR system.

To demonstrate the capability of OLFM-compensated and LHFI-amplified SPR in RI sensing, the sodium chloride (NaCl) solutions at different concentrations were prepared and measured. The real-time signal responses showed significant concentration-dependent changes (**Figure 2b**). The average voltage signals at different RIs corresponding to the solutions of various NaCl concentrations (0.01%–0.1%) were extracted and plotted (**Figure 2c**). Resolution and sensitivity are calculated by the following equation:

$$S = \frac{\Delta U}{\Delta n}$$

$$Res = \frac{U_{\text{noise}}}{S}$$

where S and Res are the sensitivity and the resolution of RI sensing, respectively. n is the RI of NaCl solution. U_{noise} is the noise value defined as three times the standard deviation of the voltage corresponding to the baseline (6.0×10^{-5} V, **Inset of Figure 2b**).

The resolution and sensitivity of OLFM-compensated and LHFI-amplified SPR system were calculated to be 5.9×10^{-8} RIU and 1.0×10^{3} V/RIU, respectively. Compared with the resolution of traditional intensity-modulated SPR system (2.0×10^{-5} RIU, **Figure S2**), that of our SPR system exhibited nearly 3 orders of magnitude enhancement of RI sensing.

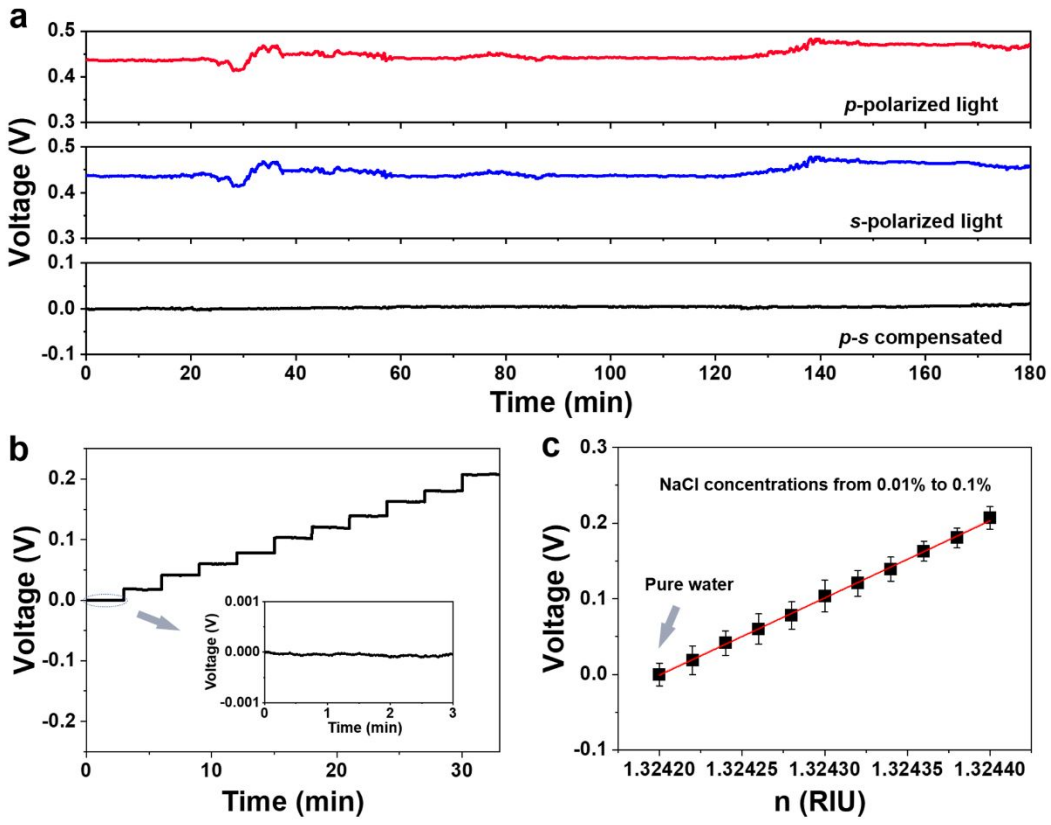

Figure 2 Performance evaluation of RI sensing. (a) The 3-hour test results of pure water; (b) Real-time signal responses with different NaCl concentrations ranging from 0.01% to 0.1%. Inset: the signal fluctuation corresponding to pure water; (c) The linear fitting curve of the voltage and the RI of NaCl solution.

Biosensing Mechanism with Universality and Versatility. In order to make the developed SPR device to be a universal biosensing platform capable of detecting a variety of analytical targets, we adopted the most common biological recognition materials and simple biosensing strategies to meet the personalized detection requirement of the target in specific scenarios. As illustrated in **Figure 1a**, nucleic acids, antibodies, and receptors acted as recognition materials to specifically interact with their targets. The presence of analytical targets triggered the surface-based binding between the target and its recognition material via direct binding or indirect competitive strategies, hence changing the RI very close to the gold film of the SPR chip, which had a quantification relationship with the target concentration. The analytical performance of RI-based biosensor is greatly reliant on the approach to anchor functional groups/molecules on the chip surface, i.e., the high-quality surface functionalization to minimum non-specific interferences, providing high target specificity. A well-established gold surface chemistry method was proposed based on the use of thiol-terminated compounds, forming SAMs on gold-coated chip via the Au-S bond (**Note S5**). In addition, in order to fully expose functional groups/molecules out of solid surface, spacer arms with different lengths are needed to design and construct by using a series of chemical reactions (**Note S3 and S4**). We adopt a rationally-designed signal readout

257 method (selected signal after buffer washing, **Note S6**) to avoid the signal disturbance
258 caused by the difference of solution RI between environmental samples.

259 **Quantification of Hg^{2+} via Using Nucleic Acid.** To test the capability of our SPR
260 system for detection of a broad range of analytical targets by adopting different
261 recognition materials, we first displayed the detection of Hg^{2+} using a Hg^{2+}-specific
262 nucleic acid sequence based on the direct binding strategy. Hg^{2+} is a well-known toxic
263 heavy metal, the detection of which is crucial for human health and ecological safety
264 protection. Ono and Togashi first reported that Hg^{2+} ions can specifically and sensitively
265 interact with two thymines for formation of a stable T–Hg^{2+}–T structure,[21] which has
266 been widely exploited to construct various Hg^{2+}-specific biosensing techniques. As
267 shown in **Figure 3a**, the Hg^{2+}-specific nucleic acid sequence introducing sulfydryl
268 group on the 5′-end with six methyl groups as the spacer arm (SH-C_6-CCC CCC TTC
269 TTT CTT CCC CCC CCC CCT TGT TTG TT) was immobilized on the SPR chip by
270 the introduction of Au-S bond (**Note S5**). The presence of Hg^{2+} caused the T–T
271 mismatch, promoting the conformation change of the sequence to form the hairpin
272 structure. The Hg^{2+}-dependent hairpin structure changed the RI very close to the gold
273 film, which was accurately captured by our SPR system. The real-time SPR signal
274 responses upon the addition of the target Hg^{2+} at different concentrations showed that
275 the signal gradually increased and reached the platform with the increased Hg^{2+}
276 concentration (**Figure 3b**). We fitted the calibration curve of signal response versus
277 target concentration by using a four-parameter logistic model (**Figure 3c**). The relative
278 standard deviations (RSDs) of triple measurement in parallel ranged from 4.7% to 9.6%,

showing satisfactory stability. The linear region, defined as 20%–80% inhibition, was observed in the range of 2.0×10^3 to 6.1×10^7 ng/L. According to the rule of 90% inhibition, the limit of detection (LOD) for Hg^{2+} approached 70 ng/L with an RSD of 6.9% (n=3). To further demonstrate the analytical performance of our device, we compared it with most previously reported Hg^{2+} biosensor based on the similar T–T mismatch strategy (**Table S1**). Our SPR system outperforms other biosensors in terms of LOD and linear range, confirming the enhanced sensitivity of intensity-modulated SPR sensing by using common-path laser heterodyne feedback.

To assess the selectivity of this method, the interference effects of seven metal ions commonly coexisted in matrix, including Ca^{2+}, Cd^{2+}, Cu^{2+}, Zn^{2+}, Pb^{2+}, Mg^{2+}, Ni^{2+} and their mixture on the signal response of this Hg^{2+}-specific nucleic acid-based biosensor were investigated under the same condition (**Figure 3d**). In these experiments, all metal ions were spiked at a final concentration of 1.5×10^3 nM, i.e., EC_{50}, approximately the inflection of standard curve reflecting approximately 50% of the maximum possible response for the target (**Figure 3c**). Except for Hg^{2+}, we observed that the signals of other eight interfering ions were indistinguishable from the blank group, indicating that the good selectivity of the SPR biosensor. On the contrary, the signals in response to Hg^{2+} at both concentrations of 1.0×10^5 and 1.0×10^6 ng/L were negligible if the SPR chip was not functionalized with Hg^{2+}-specific nucleic acid sequences (**Figure S3**).

In addition, the intra-assays (five groups synthesized in the same batch) and inter-assays (synthesized in five batches) of the as-prepared Hg^{2+}-specific nucleic acid functionalized SPR chip were evaluated at the Hg^{2+} concentration of 1.5×10^3 nM. The

RSDs were 5.45% and 8.08% for intra- and inter-assays, respectively (**Figure 3e**), indicating the good reproducibility and batch-to-batch precision of the gold surface chemistry for nucleic acid functionalization.

We evaluated the analytical performance of biosensor for Hg^{2+} in different matrix, including tap and bottled water. The average recoveries were in the range of 95% to 112% with the acceptable RSDs within 10% in three concentration levels-spiked samples (**Table S2**), suggesting that this technique exhibited satisfactory accuracy for Hg^{2+} detection in water matrix.

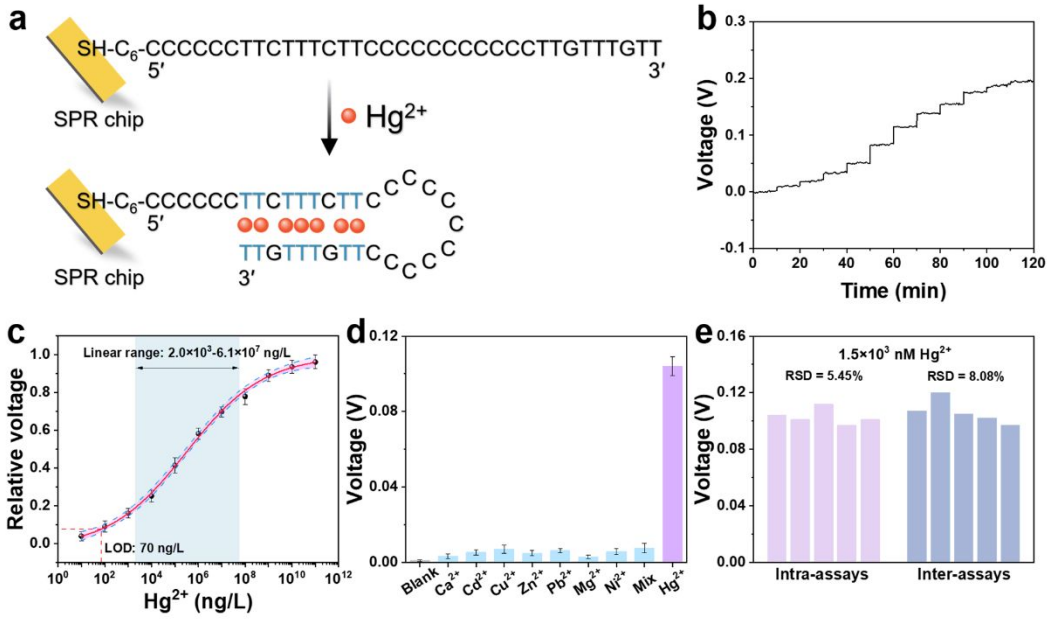

Figure 3 Performance evaluation of Hg^{2+}-specific nucleic acid-based biosensor. (a) Schematic diagram of sensing mechanism for Hg^{2+}; (b) Signal responses in real-time with various Hg^{2+} concentrations from 10^{1} to 10^{11} ng/L (adding the Hg^{2+} from low to high concentrations); (c) Standard curve for Hg^{2+} detection fitted with a four-parameter logistic model. Relative voltage means the ratio of the voltage of different Hg^{2+} concentrations to the fitted maximum voltage in the four-parameter logistic model; (d)

316 Selectivity of Hg^{2+} detection against other interfering metal ions at the same
317 concentrations of 1.5×10^3 nM. The blank group was the biosensor signal responding to
318 phosphate buffered saline solution; (e) Batch-to-batch intra-assays precision and inter-
319 assays reproducibility of this biosensor.

320 **Broad-spectrum Immunoassay for Microcystins.** We further tested the capability of
321 our SPR system to variant-independently detect MCs based on a self-produced group-
322 specific monoclonal antibody presenting both broad-spectrum recognition capabilities
323 and high affinities against MCs.[22] MCs are a group of cyclic heptapeptide cyanotoxins
324 with more than 150 variants, being of high toxicity and broad distribution due to the
325 intensified algal blooming events in lakes, and their common routes of exposure include
326 ingestion of contaminated drinking water, food, and algal feed supplements.
327 Considering that the low-molecular-weight MCs targets are hard with different epitopes
328 for the commonly used sandwich immunoassay, we adopted the indirect competitive
329 mode for MCs detection (**Figure 4a**), in which we prepared the BSA−microcystin-LR
330 (BSA−MC-LR) conjugates (**Note S3**) and formed SAMs on the SPR surface via the Au-
331 S bond by introducing a bifunctional crosslinker 11-MUA (**Note S5**). The samples
332 containing MCs were preincubated with the MCs-specific antibody solution to generate
333 the antibody−antigen interaction, and then fed into the sensing unit, so that the unreacted
334 antibody interacted with the immobilized MC-LR on the chip surface, resulting in the
335 changes of RI at the interface. The higher concentrations of MCs in samples would
336 induce the smaller RI change, hence exhibiting a typical "turn-off" sensing mode.

337 The antibody concentration is a critical factor affecting the analytical performance of

indirect competitive immunoassay. We tested the effect of various concentrations of antibody in the range of 0.01 to 10 μg/mL on the signal response and found that the signals increased with the increased antibody concentrations (**Figure S4**). The signals at different antibody concentrations fitted by the four-parameter logistic model demonstrated that the antibody concentrations ranging from 1 to 10 μg/mL represented a sensitive linear region with proportional signal change. To save testing cost, 1.0 μg/mL antibody was selected as the optimal one for use. As a proof-of-concept, the real-time gradient signal responses towards MC-LR, one variant of MCs, at various concentrations ranging from 10^{-1} to 10^{5} ng/L were recorded (**Figure 4b**), and the corresponding standard curve was fitted by the logistic model (**Figure 4c**), achieving a LOD of 3.9 ng/L with a linear region from 13 to 1010 ng/L. The ultralow limit detection is nearly 3 orders of magnitude lower than the defined maximal total MCs in drinking water, i.e., 1000 ng/L set by the World Health Organization (WHO).[23] In addition, our biosensor was nearly 2 orders of magnitude sensitive than some commercialized detection techniques such as ENZO MCs enzyme-linked immunosorbent assay (ELISA) kit (LOD up to 100 ng/L)[24] with simple and time-saving operating procedures.

To assess the broad-spectrum specificity of this biosensor towards MCs, we tested the signal responses of five MC variants, including MC-LR, microcystin-YR (MC-YR), microcystin-LY (MC-LY), microcystin-WR (MC-WR), and microcystin-LA (MC-LA) at 0.1 nM, i.e., EC_{50} in **Figure 4c**, to see the slightest signal difference in the most sensitive range. Besides, considering that the Adda residue of MCs containing benzene ring is the likely antigenic epitope, hence contributing greatly to the orientation in the

binding interaction with the group-specific antibody,[22] we also tested the selectivity of this biosensor toward 2,4-dichlorophenoxyacetic acid (2,4-D) and bisphenol A (BPA), both of that contain benzene rings. As expected, all five MC variants showed lower signal responses than that of the blank group due to the "turn-off" sensing mode (**Figure 4d**). However, the presence of neither BPA nor 2,4-D produced obvious signal change compared with the blank group, indicating that our biosensor was highly selective for MCs. Besides, the gold surface chemistry for protein functionalization also exhibited good reproducibility and batch-to-batch precision within 6.2% of RSDs (**Figure S5**). We measured the lake water samples spiked with 1.0×10^3, 1.0×10^4 and 1.0×10^5 ng/L of MC-LR, respectively, by using the biosensor and the ELISA method recommended by the U.S. Environmental Protection Agency. We observed that the average recoveries ranged from 89% to 118% with acceptable RSDs less than 10% (n=5) measured by the biosensor (**Table S3**), and both results showed the positive correlation with a strong linear relationship (r^2=0.997) (**Figure 4e**).

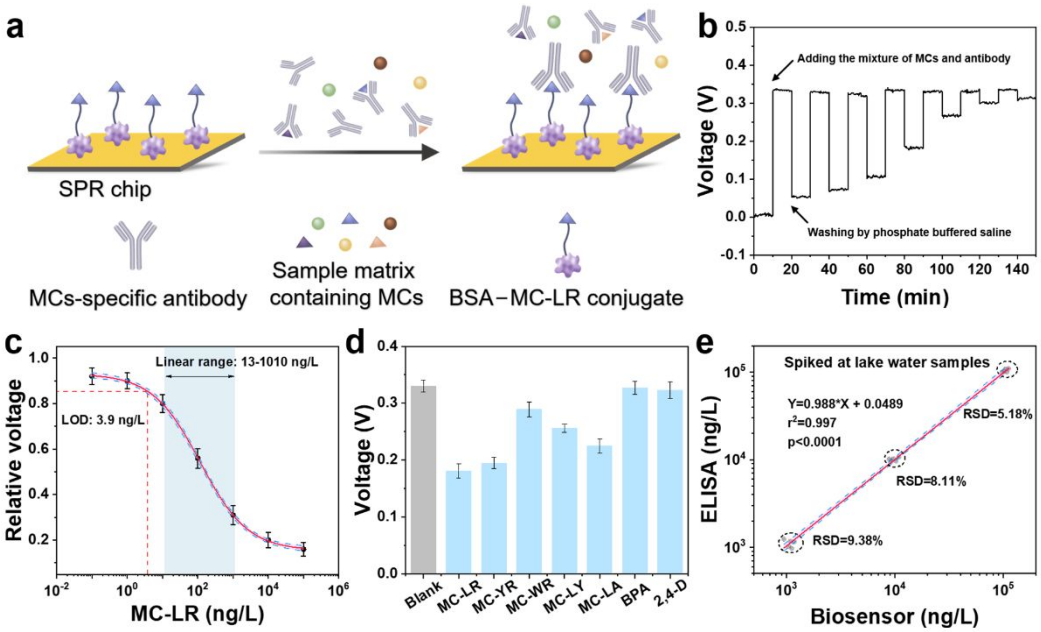

Figure 4 Performance evaluation of MCs-specific antibody-based biosensor. (a) Schematic diagram of sensing mechanism for MCs; (b) Signal responses in real-time with various MCs concentrations from 10^{-1} to 10^{5} ng/L (adding the MCs from high to low concentrations); (c) Standard curve for MC-LR detection fitted by a four-parameter logistic model as a proof-of-concept. Relative voltage means the ratio of the voltage with different MC-LR concentrations to the voltage without the addition of MC-LR; (d) Signal responses towards MC variants and other compounds at the same concentrations of 0.1 nM. The signal response to phosphate buffered saline solution was defined as the blank group; (e) Correlation analysis of the detection results between our biosensor and the standard ELISA method for the spiked MC-LR in lake waters.

Screening of Estrogenic Binding Activity in WWTP. Lastly, we evaluated the capability of our SPR system for screening natural and environmental estrogens by using a nuclear hormone receptor. Natural estrogens have long been known to be the major sex steroid hormones regulating the development and function of reproductive

organs as well as other functions. Environmental estrogens can mimick the action of the natural estrogens or disturb the signal transduction pathways of estrogens, hence producing the deformity of reproductive system. The affinity interaction between estrogens and nuclear estrogen receptors (nERs) is recognized as one of the molecular initiative events of estrogen signal transduction pathways.[3, 25] Inspired by this affinity interaction, we designed an indirect competitive-binding assay for screening of estrogenic binding activity (**Figure 5a**). As similar as in **Figure 4a**, we prepared the BSA−17β-estradiol (BSA−E_2) conjugates (**Note S4**) and functionalized the conjugates on the chip surface (**Note S5**). The sample containing estrogenic binding activity was preincubated with the recombined human estrogen receptor α ligand binding domain (hERα-LBD), which was described in our previous work.[26] The unbound hERα-LBD fed into the sensing unit was then interacted with the immobilized E_2 on the chip surface. And the hERα-LBD induced RI change on the chip surface was accurately captured by the SPR system in a "turn-off" sensing mode.

After optimizing the concentrations of hERα-LBD which are critical factors influencing the analytical performance (**Figure S6**), 2.5 μg/mL hERα-LBD were selected considering both sensitivity and testing cost. We took E_2 as the representative estrogen and recorded the real-time SPR signal responses at various concentrations ranging from 10^{-1} to 10^5 ng/L (**Figure 5b**), and fitted the standard curve (**Figure 5c**). The LOD for E_2 reached 0.7 ng/L with a linear range from 4 to 967 ng/L. We compared the LOD of this method with that of a variety of estrogen receptor-based techniques applied for screening of estrogenic binding activity (**Figure 5d**). Our biosensor outperformed others

411 using different transducers such as piezoelectric,[27] fluorescent,[28] nonisotopic,[29] SPR,[30]
412 the standard ELISA method,[31] and commercial estrogenic binding activities kit.[32]
413 Compared with many cell-based in vitro assays based on the same binding mechanism
414 between estrogens and nERs, such as ER-CALUX®,[33] E-Screen assay,[34] and the Yeast
415 Estrogen Screen (YES) assay,[35] our estrogen receptor-based SPR biosensor not only has
416 obvious sensitivity advantage, but also is cell-free and unaffected by the cytotoxic
417 substances in matrices, especially in environmental samples, hence endowing with
418 satisfactory accuracy and stability.

419 In order to validate the practicability of the developed SPR biosensor, the wastewater
420 samples collected from a WWTP in Tsinghua Campus along treatment processes were
421 tested (**Figure S7**). The wastewater samples, including influent samples and effluent
422 samples, was divided into two groups. One group was directly measured by the
423 developed biosensor after simple filtration, and the other group was enriched by solid-
424 phase extraction (SPE) method and then were diluted to the initial concentration with
425 binding buffer before detection. The estrogenic binding activity of wastewater samples
426 was characterized using E_2-binding activity equivalent (E_2-BAE). As shown in **Figure**
427 **5e**, the influent and effluent samples were 35−128 and 0−9.8 ng/L E_2-BAE, respectively,
428 which was similar to the previously reported results from WWTPs in China, European,
429 and America.[36-38] The estrogenic binding activities of influent samples were
430 significantly lower than that of effluent samples, which could be attributed to the high
431 removal efficiency of estrogen-active compounds during biodegradation process, such
432 as 89% E_2.[39] In addition, the estrogenic binding activities of wastewater samples without

SPE were slightly higher than those with SPE, which was easy to understand that there may be some loss during the extraction and elution process. And the two results exhibited a good linear relationship (broken lines in **Figure 5e**), illustrating that the developed SPR biosensor could accurately and reliably detect estrogenic binding activity in complex wastewater samples without the need for enrichment. We attribute this great advantage to the ultrasensitivity and the rationally-designed signal readout method of our SPR system, which can well resist the interference of matrix effect. Therefore, the SPR biosensor has satisfactory performance for screening of estrogenic binding activities in real samples.

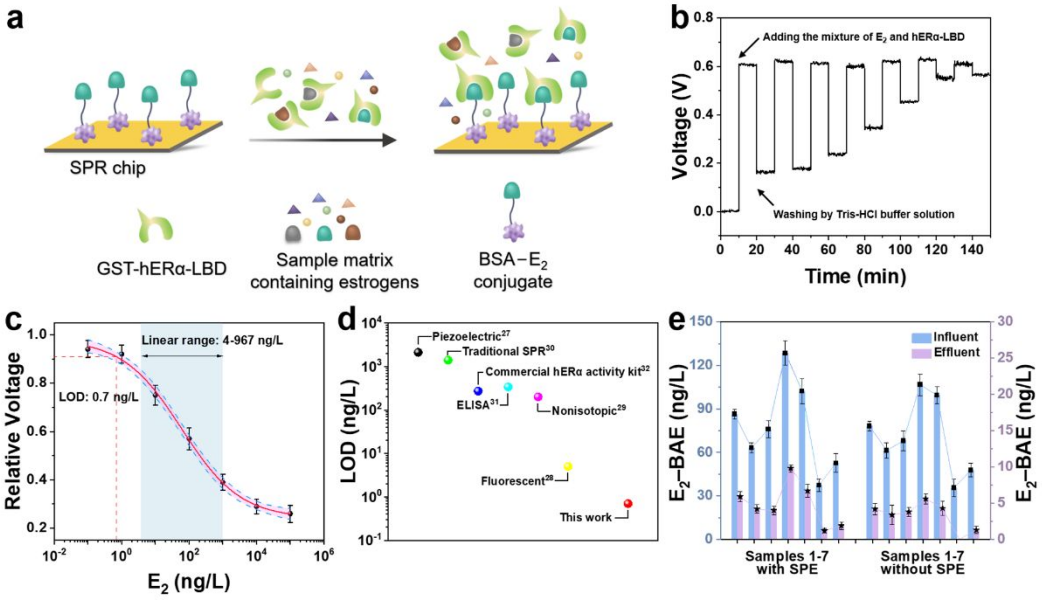

Figure 5 Performance evaluation of estrogen-specific receptor-based biosensor. (a) Schematic diagram of sensing mechanism for estrogens; (b) Signal responses in real-time with various concentrations of E_2 from 10^{-1} to 10^5 ng/L (adding the E_2 from high to low concentrations); (c) Standard curve for estrogenic binding activity detection fitted by a four-parameter logistic model by taking E_2 as a proof. Relative voltage means the ratio of the voltage with different E_2 concentrations to the voltage without the addition

of E_2; (d) Comparison of LOD of our SPR biosensor with other estrogen receptor-based biosensors. The numbers represent the corresponding references in the article; (e) Estrogenic binding activities assay of wastewater samples from the WWTP with and without SPE detected by the biosensor. 1–7 represent samples for 7 days within a week. The E_2-BAE of the influent samples corresponding to the blue scale (left) and that of the effluent samples corresponding to the red scale (right).

ENVIRONMENTAL IMPLICATIONS

This work proposed a polarized light-compensated SPR system with laser heterodyne feedback, resulting in nearly 3 orders of magnitude enhancement of sensitivity over the original SPR system. It utilizes the laser source acting as the emitter, responder, and intrinsic amplifier simultaneously, rarely need optical alignment, and reduces the optical components required, providing a solid research foundation for the development of portable and efficient optical detection devices. In addition, a common-path compensation approach combines the orthogonally-polarized light with frequency multiplexing to resist the interference from environmental noise, which is expected to meet the requirements of on-site inspection.

Based on different recognition materials, the SPR system could achieve the ultrasensitive detection of a variety of analytical targets, from a single small molecule, to a group of chemicals with general structure and their isomers, and to a class of effect-targeting endocrine disrupting activity. Compared with our previous evanescent wave fluorescence biosensor,[28] the ultrasensitivity and rationally-designed signal readout method of this SPR system can effectively avoid the interference of matrix effect in

complex environmental samples, thus greatly reducing or even avoiding the time consumed by sample concentration, extraction, and enrichment to achieve rapid detection. As a stable and reliable SPR biosensor with ultrasensitivity and universality, it holds promise to revolutionize environmental monitoring, medical diagnostics, and food safety, and provides methodological support for safeguarding environmental and public health.

ASSOCIATED CONTENT

Supporting Information

The Supporting Information is available free of charge at https://pubs.acs.org/doi/10.1021/acs.est.xxxxxxx.

Detailed information on materials and reagents, transfer matrix method, synthesis procedures of BSA−MC-LR and BSA−E_2 conjugates, gold surface chemistry, quantification procedures, and sample collection and pretreatment are provided in the **Supporting Information**.

AUTHOR INFORMATION

Corresponding Author

Xiaohong Zhou – State Key Joint Laboratory of ESPC, School of Environment, Tsinghua University, Beijing 100084, China; orcid.org/0000-0002-5307-6709; Email: xhzhou@mail.tsinghua.edu.cn

Yidong Tan – State Key Laboratory of Precision Measurement Technology and Instruments, Department of Precision Instrument, Tsinghua University, Beijing, 100084,

China; orcid.org/0000-0002-9906-7875; Email: Tanyd@mail.tsinghua.edu.cn

Authors

Jisui Tan – State Key Joint Laboratory of ESPC, School of Environment, Tsinghua University, Beijing 100084, China

Zongren Dai – State Key Laboratory of Precision Measurement Technology and Instruments, Department of Precision Instrument, Tsinghua University, Beijing, 100084, China

Kaiming Zhou – Aston Institute of Photonic Technologies, Aston University, Birmingham B4 7ET, UK

Lin Zhang – Aston Institute of Photonic Technologies, Aston University, Birmingham B4 7ET, UK

Miao He – State Key Joint Laboratory of ESPC, School of Environment, Tsinghua University, Beijing 100084, China

Notes

The authors declare to no competing financial interest.

Acknowledgements

We acknowledge support from the Newton Advanced Fellowship of Royal Society under Grant 191072, the National Key Research and Development Project under Grant 2022YFF0609100, and the National Natural Science Foundation of China under Grant 21976100 and 51961130387.

REFERENCES

1. Minopoli, A.; Della Ventura, B.; Lenyk, B.; Gentile, F.; Tanner, J. A.; Offenhäusser, A.; Mayer, D.; Velotta, R., Ultrasensitive antibody-aptamer plasmonic biosensor for malaria biomarker detection in whole blood. *Nat. Commun.* **2020**, *11*, 6134.
2. Xiang, Y.; Lu, Y., Using personal glucose meters and functional DNA sensors to quantify a variety of analytical targets. *Nat. Chem.* **2011**, *3*, 697-703.
3. Brzozowski, A. M.; Pike, A. C. W.; Dauter, Z.; Hubbard, R. E.; Bonn, T.; Engström, O.; Öhman, L.; Greene, G. L.; Gustafsson, J.-Å.; Carlquist, M., Molecular basis of agonism and antagonism in the oestrogen receptor. *Nature* **1997**, *389*, 753-758.
4. Chen, Y.; Liu, J.; Yang, Z.; Wilkinson, J. S.; Zhou, X., Optical biosensors based on refractometric sensing schemes: A review. *Biosens. Bioelectron.* **2019**, *144*, 111693.
5. Wijaya, E.; Lenaerts, C.; Maricot, S.; Hastanin, J.; Habraken, S.; Vilcot, J.-P.; Boukherroub, R.; Szunerits, S., Surface plasmon resonance-based biosensors: From the development of different SPR structures to novel surface functionalization strategies. *Curr. Opin. Solid State Mater. Sci.* **2011**, *15*, 208-224.
6. Suzuki, A.; Kondoh, J.; Matsui, Y.; Shiokawa, S.; Suzuki, K., Development of novel optical waveguide surface plasmon resonance (SPR) sensor with dual light emitting diodes. *Sens. Actuators B Chem.* **2005**, *106*, 383-387.
7. Liu, L.; Ye, K.; Lin, C.; Jia, Z.; Xue, T.; Nie, A.; Cheng, Y.; Xiang, J.; Mu, C.; Wang, B.; Wen, F.; Zhai, K.; Zhao, Z.; Gong, Y.; Liu, Z.; Tian, Y., Grain-boundary-rich polycrystalline monolayer WS2 film for attomolar-level Hg2+ sensors. *Nat. Commun.* **2021**, *12*, 3870.
8. Law, W.-C.; Markowicz, P.; Yong, K.-T.; Roy, I.; Baev, A.; Patskovsky, S.; Kabashin, A. V.; Ho, H.-P.; Prasad, P. N., Wide dynamic range phase-sensitive surface plasmon resonance biosensor based on measuring the modulation harmonics. *Biosens. Bioelectron.* **2007**, *23*, 627-632.
9. Zijlstra, P.; Paulo, P. M. R.; Orrit, M., Optical detection of single non-absorbing molecules using the surface plasmon resonance of a gold nanorod. *Nat. Nanotechnol.* **2012**, *7*, 379-382.
10. Lacot, E.; Day, R.; Stoeckel, F., Laser optical feedback tomography. *Opt. Lett.* **1999**, *24*, 744-746.
11. Zhu, K.; Guo, B.; Lu, Y.; Zhang, S.; Tan, Y., Single-spot two-dimensional displacement measurement based on self-mixing interferometry. *Optica* **2017**, *4*, 729-735.
12. Wang, Y.; Xu, X.; Dai, Z.; Hua, Z.; Lin, C.; Hou, Y.; Zhang, Q.; Wang, P.; Tan, Y., Frequency-swept feedback interferometry for noncooperative-target ranging with a stand-off distance of several hundred meters. *PhotoniX* **2022**, *3*, 21.
13. Ohtomo, T.; Sudo, S.; Otsuka, K., Detection and counting of a submicrometer particle in liquid flow by self-mixing microchip Yb:YAG laser velocimetry. *Appl. Opt.* **2016**, *55*, 7574-7582.
14. Mowla, A.; Du, B. W.; Taimre, T.; Bertling, K.; Wilson, S.; Soyer, H. P.; Rakić, A. D., Confocal laser feedback tomography for skin cancer detection. *Biomed. Opt. Express* **2017**, *8*, 4037-4048.
15. Wan, X.; Li, D.; Zhang, S., Quasi-common-path laser feedback interferometry based on frequency shifting and multiplexing. *Opt. Lett.* **2007**, *32*, 367-369.
16. Wu, T.; Shen, J.; Li, Z.; Zou, T.; Xin, W.; Xing, F.; Zhang, F.; Man, Z.; Fu, S., Graphene-based ultrasensitive optical microfluidic sensor for the real-time and label-free monitoring of simulated arterial blood flow. *Opt. Express* **2020**, *28*, 16594-16604.
17. Xu, X.; Dai, Z.; Wang, Y.; Li, M.; Tan, Y., High Sensitivity and Full-Circle Optical Rotary Sensor for Non-Cooperatively Tracing Wrist Tremor With Nanoradian Resolution. *IRE Trans. Ind. Electron.* **2022**, *69*, 9605-9612.
18. Zhu, K.; Chen, H.; Zhang, S.; Shi, Z.; Wang, Y.; Tan, Y., Frequency-Shifted Optical Feedback

Measurement Technologies Using a Solid-State Microchip Laser. *Appl. Sci.* **2019**, *9*, 109.
19. Donati, S., Developing self-mixing interferometry for instrumentation and measurements. *Laser Photonics Rev.* **2012**, *6*, 393-417.
20. Ma, G.; Liang, R.; Wan, Z.; Wang, S., Critical angle reflection imaging for quantification of molecular interactions on glass surface. *Nat. Commun.* **2021**, *12*, 3365.
21. Akira; Ono; Humika; Togashi, Highly Selective Oligonucleotide-Based Sensor for Mercury(II) in Aqueous Solutions. *Angew. Chem.* **2004**, *116*, 4400-4402.
22. Liu, J.; Yang, Y.; Zhu, Q.; Wang, Z.; Hu, G.; Shi, H.; Zhou, X., ELISA-Based Method for Variant-Independent Detection of Total Microcystins and Nodularins via a Multi-immunogen Approach. *Environ. Sci. Technol.* **2021**, *55*, 12984-12993.
23. Organization, W. H. Guidelines for drinking-water quality: fourth edition incorporating the first and second addenda. https://www.who.int/publications/i/item/9789240045064 (accessed by February 17, 2022).
24. Enzo Life Sciences, I. Microcystins (Adda specific) ELISA kit[EB/OL]. https://www.enzolifesciences.com/ALX-850-319/microcystins-adda-specific-elisa-kit/ (accessed by February 17, 2022).
25. Zacharewski, In Vitro Bioassays for Assessing Estrogenic Substances. *Environ. Sci. Technol.* **1997**, *31*, 613-623.
26. Liu, L.; Zhou, X.; Lu, Y.; Shan, D.; Xu, B.; He, M.; Shi, H.; Qian, Y., Facile screening of potential xenoestrogens by an estrogen receptor-based reusable optical biosensor. *Biosens. Bioelectron.* **2017**, *97*, 16-20.
27. Zhihong, M.; Xiaohui, L.; Weiling, F., A new sandwich-type assay of estrogen using piezoelectric biosensor immobilized with estrogen response element. *Anal. Commun.* **1999**, *36*, 281-283.
28. Tan, J.; Liu, L.; Li, F.; Chen, Z.; Chen, G. Y.; Fang, F.; Guo, J.; He, M.; Zhou, X., Screening of Endocrine Disrupting Potential of Surface Waters via an Affinity-Based Biosensor in a Rural Community in the Yellow River Basin, China. *Environ. Sci. Technol.* **2022**, *56*, 14350-14360.
29. Garrett, S. D.; Lee, H. A.; Morgan, M. R. A., A nonisotopic estrogen receptor–based assay to detect estrogenic compounds. *Nat. Biotechnol.* **1999**, *17*, 1219-1222.
30. Habauzit, D.; Armengaud, J.; Roig, B.; Chopineau, J., Determination of estrogen presence in water by SPR using estrogen receptor dimerization. *Anal. Bioanal. Chem.* **2008**, *390*, 873-883.
31. Wang, Y.; Wang, M.; Zhou, L.; Geng, X.; Xu, Z.; Zhang, H., Development of a competitive ELISA based on estrogen receptor and weak competitive molecule for the screening of potential estrogens in foods. *Food Chem.* **2023**, *401*, 134084.
32. Beijing Campus Technology Co., Ltd. http://www.bjkbc-tech.com/ (accessed by February 17, 2022).
33. Van der Linden, S. C.; Heringa, M. B.; Man, H.-Y.; Sonneveld, E.; Puijker, L. M.; Brouwer, A.; van der Burg, B., Detection of Multiple Hormonal Activities in Wastewater Effluents and Surface Water, Using a Panel of Steroid Receptor CALUX Bioassays. *Environ. Sci. Technol.* **2008**, *42*, 5814-5820.
34. Xin, Y.; Wan, B.; Yu, B.; Fan, Y.; Chen, D.; Guo, L.-H., Chlorinated Polyfluoroalkylether Sulfonic Acids Exhibit Stronger Estrogenic Effects than Perfluorooctane Sulfonate by Activating Nuclear Estrogen Receptor Pathways. *Environ. Sci. Technol.* **2020**, *54*, 3455-3464.
35. Stanford, B. D.; Weinberg, H. S., Evaluation of On-Site Wastewater Treatment Technology to Remove Estrogens, Nonylphenols, and Estrogenic Activity from Wastewater. *Environ. Sci. Technol.*

2010, *44*, 2994-3001.
36. Guo, W.; Li, J.; Luo, M.; Mao, Y.; Yu, X.; Elskens, M.; Baeyens, W.; Gao, Y., Estrogenic activity and ecological risk of steroids, bisphenol A and phthalates after secondary and tertiary sewage treatment processes. *Water Res.* **2022**, *214*, 118189.
37. Islam, R.; Yu, R. M. K.; Andrew-Priestley, M.; Smith, N.; Rahman, M. M.; Tran, T. K. A.; Connor, W. A. O.; MacFarlane, G. R., Secondary treatment phase of tertiary wastewater treatment works significantly reduces estrogenic load. *Water Res.* **2021**, *200*, 117257.
38. Välitalo, P.; Perkola, N.; Seiler, T.-B.; Sillanpää, M.; Kuckelkorn, J.; Mikola, A.; Hollert, H.; Schultz, E., Estrogenic activity in Finnish municipal wastewater effluents. *Water Res.* **2016**, *88*, 740-749.
39. Yang, W.; Zhou, H.; Cicek, N., Removal mechanisms of 17β-estradiol and 17α-ethinylestradiol in membrane bioreactors. *Water Sci. Technol.* **2012**, *66*, 1263-1269.